Int. J. Electrochem. Sci., 13 **(2018)** 7949 – 7967, doi: 10.20964/2018.08.13

International Journal of ELECTROCHEMICAL SCIENCE
www.electrochemsci.org

Corrosion Evaluation of Pipeline Steel API 5L X52 in partially deaerated Produced Water with High Chloride Content

Natalya V. Likhanova[1], *Noel Nava*[1], *O. Olivares-Xometl*[2,*] , *M.A. Domínguez-Aguilar*[1], *P Arellanes-Lozada*[2], *Irina V. Lijanova*[3], *Janette Arriola-Morales*[2], *Luis Lartundo-Rojas*[4].

[1] Instituto Mexicano del Petróleo, Eje Central Lázaro Cárdenas No. 152, Col. San Bartolo Atepehuacan, México D.F. 07730, México.
[2] Benemérita Universidad Autónoma de Puebla, Facultad de Ingeniería Química, Av. San Claudio, Ciudad Universitaria. Col. San Manuel, Puebla, Pue. 72570, México.
[3] Instituto Politécnico Nacional, CIITEC, Cerrada Cecati S/N, Colonia Santa Catarina, Azcapotzalco, México D.F. 02250, México.
[4] Instituto Politécnico Nacional, Centro de Nanociencias y Micro y Nanotecnologías, UPALM, Zacatenco, México D.F. CP. 07738, México
[*]E-mail: oxoctavio@yahoo.com.mx

Received: 17 March 2018 / *Accepted:* 14 May 2018 / *Published:* 5 July 2018

The corrosion mechanism of pipeline steel X52 exposed to produced water is proposed based on identified chemical species and scale after 270 days. Polarization curve profiles suggested that steel corrosion products are formed and removed periodically. X-ray diffraction, Mössbauer and Ultraviolet-visible spectroscopies identified akaganeite/lepidocrocite ($Fe^{3+}O(OH)$) along with goethite (α-FeOOH) and magnetite (Fe_3O_4) as a result of iron oxidation in water to conform an external layer. XPS detected the presence of $FeCl_2$ and $Fe_2(SO_4)_3$ in the internal layer derived from previous adsorption on the surface. SEM indicated the presence of general and localized corrosion under corrosion products.

Keywords: Pipeline steel; Corrosion behavior; Produced water; Surface analysis; Electrochemical techniques.

1. INTRODUCTION

Water is normally associated with hydrocarbon production operations as it is naturally contained in oil basins. Formation water (FW) exists in the rocks before drilling and contains a variety of organic and inorganic dissolved compounds. This water is considered as the most corrosive environment in oil field operations since carbon dioxide (CO_2) and hydrogen sulfide (H_2S) are present, in addition to other aggressive compounds such as sulfates and chlorides. Oxygen can also enter the sour system as a trace element. FW obtained from reservoirs is composed of subjacent aquifer, connate

and injection waters [1, 2]. The chemical composition of FW depends on the nature of the geological formation along with the hydrocarbon reservoir depth [3-6]. However, it is clear that the chemical composition of FW turns water into a corrosive medium [7-9]. Hydrocarbon extraction is accompanied by oil, gas and produced water; the latter containing organic acids and various dissolved gases (CO_2, H_2S) whose concentrations are unique depending on the formation [10, 11]. After crude oil production, water can be disposed or reinjected to keep the reservoir pressure and favor a reduction in oil production costs [12, 13]. In secondary oil recovery operations, raw sea water is commonly injected into the well formation to displace oil and bring it to the surface. This water contains acid gases and inorganic salts and it is enriched with oxygen so it is denominated produced water (PW). Equipment and pipelines, commonly made of carbon steels, are likely to be corroded in these environments, which may lead to substantial economic losses and human casualties [14, 15]. Chloride and sulfate ions accelerate the aqueous corrosion of carbon steel pipelines [16]. CO_2 is particularly corrosive, especially in some produced brines containing aggressive ions such as chlorides (Cl^-) and sulfates (SO_4^{2-}) [17]. Likewise, weak organic acids such as acetic, formic and propionic acids are commonly present in oil brines within 500-3000 ppm, so trace amounts are likely to increase the corrosivity of produced water [18]. It is well known that most corrosion studies related to FW are performed in synthetic brines: Mansoori *et al*. [19] carried out a corrosion study in API 5L X65 steel, which transported natural gas and gas condensates (naphtha) in combination with free water and oxygen; although the reported corrosion rate was relatively low (~2 mpy^{-1}), the steel surface displayed pitting corrosion. Choi *et al*. [20] completed studies to determine the mutual solubility of water/carbon dioxide/water for different combinations of pressure, concentration and temperature so as to simulate water-gas transmission. These authors reported that the CO_2 solubility in water decreased by increasing temperature and concentration while water salinity was constant; notwithstanding, the corrosion damage was evident. Other studies performed on carbon steel in PW with synthetic brines saturated with CO_2 were done by Zhang and Cheng [21, 22] in order to establish the type of corrosion occurring on steel in this medium. Oxygen plays an important role in aqueous steel corrosion when in presence of minor contents of acid gases. The O_2 and H_2S interactions promoted the formation of elemental sulfur whose dissolution in water may lead to FeS, Fe_2O_3, FeOOH and S [23]. Likewise, the presence of O_2 and SO_2 may result in the formation of sulfuric acid, which increases water corrosivity and induces the formation of $FeSO_4 \cdot 4H_2O$, FeOOH, and $FeSO_3xH_2$ scales [24]. The presence of oxygen increases the corrosion rate of carbon steel in aqueous CO_2 and decreases the efficiency of corrosion inhibitors in acidic environments [25, 26]. The contribution of oxygen corrosion in brine solutions is additive to natural corrosion. Likewise, the presence of oxygen can affect corrosion products, transforming stable products such as mackinawite ($Fe_{1-x}S$) into metastable greigite (Fe_3S_4) whose film is dissolved and corrosion increased [27]. These articles claim that the corrosion process occurring in metals in either PW or synthetic media is complex. Moreover, PW does not always preserve dissolved gases such as CO_2 or H_2S though water contains a large content of dissolved salts as oil reservoirs are normally adjacent to saline domes; similarly, temperature and operation activities allow oxygen contamination and gas desorption. A test program of carbon steel under static/dynamic conditions in partially deaerated seawater with travels up to 1 ppm O_2 indicated the presence of general corrosion, which was exacerbated under flowing conditions, so carbon steel might reach 1.25 mmy^{-1}

[28]. Pitting corrosion normally occurs on carbon steel under aerated conditions at room temperature within the pH interval from 4 to 12 [29, 30]. Halide ions such as Cl^- and Br^- exert a relevant effect on localized corrosion, which is worsened in the presence of oxygen as temperature accelerates the kinetics of corrosion reactions [30, 31]. Most of the cited studies were done in synthetic brines saturated with carbon dioxide. This work is focused on the corrosion process of pipeline steel X52 exposed to PW for long periods of time (a maximum of 270 days), which was turned to be aerated with 2 ppm of oxygen when extracted; additional tests at 25 and 45 °C were run. Polarization scans along with surface analyses by scanning electron microscopy (SEM/EDX) and X-ray photoelectron spectroscopy (XPS) were performed to observe long term corrosion behavior of steel in the saline environment. The corrosion products were characterized by Mössbauer spectroscopy, diffuse reflectance ultraviolet-visible spectroscopy (DRUV) and X-ray diffraction (XRD) to correlate test parameters.

2. MATERIALS AND METHODS

2.1. Preparation of materials

Tests were carried out on API 5L X52 steel blanks with the following chemical composition (wt.%): 0.06 C, 0.6 Si, 0.7 Mn, 0.005 P, 0.001 S, 0.012 Ni, 0.015 Cr, 0.04 Mo, 0.02 V, and 0.02 Cu balanced with iron. Specimens were wet abraded with silicon carbide paper (number 240-2000), degreased in hexane and washed in an ultrasonic acetone bath to remove impurities. Electrochemical and SEM-EDX tests were performed in an area of 0.283 cm^2. Steel samples with dimensions of 1.0 cm × 1.0 cm × 0.5 cm were used for XPS analyses. The collection of corrosion products for the Mössbauer spectroscopy was performed in samples of 5.08 cm × 2.54 cm × 2.54 cm.

2.2. Test solution

The test solution consisted of water samples coming from an oil well located in the south west of Mexico. PW was characterized by the inductively coupled plasma (ICP) method as described elsewhere [32, 33]. PW was mainly composed of anions in the form of chlorides, sulfates and nitrates whereas cations included sodium, calcium, magnesium and strontium as shown in Table 1.

Table 1. Chemical composition of oilfield PW by Steve & Davis´ analysis

Anions	**F^-**	**Cl^-**	**Br^-**	**NO_2^-**	**HCO^{3-}**		**SO^{4-}**
Concentration (g L^{-1})	0.444	166.7	1.6	<0.0001	2.4		0.4
Cations	**Fe**	**$CaCO^{3+}$**	**$MgCO^{3+}$**	**Na^+**	**K^+**	**Ba**	**Sr**
Concentration (g L^{-1})	0.02	41.2	57.7	61.7	0.86	0.32	1.3
pH	**Conductivity (µS cm^{-1})**			**Dissolved oxygen concentration (ppm)**			
4.8	218 000 a 20 °C			2			

The Stiff & Davis´ analysis established that Na^+ (61.7 g l^{-1}) and Cl^- (166.7 g l^{-1}) predominated in water. A stability index of 1.24 was determined, which along with the bicarbonate content, suggested that PW might scale. However, a low pH of 4.8 made corrosion the predominant feature.

PW can be highly corrosive depending on pH, chlorides, organic acids, oxygen and temperature as these factors boost corrosion. Likewise, halide ions contained in PW are highly active and destroy "passivity" so mild steel may become susceptible to pitting corrosion [31].

2.3. Analysis of corrosion products by experimental techniques

XPS analyses were performed on a spectrometer equipped with a Kα X-ray source of 1486 eV. The analyzer energy was 23.5 eV at a base pressure of 4.5 x 10^{-8} Pa. The analyzed samples were immersed in PW for 60 days at 25 °C. The obtained spectra were adjusted to the C 1s (284.6 eV) peak. The identification of the chemical species was performed by fitting the spectrum curves to a Gaussian distribution. The high resolution spectra were assigned to the corresponding species through a deconvolution procedure. Micrographs were obtained in a SEM JEOL-JSM-6300 equipped with an energy dispersive spectrometry module. The analyzed surfaces were exposed to PW for 90, 180 and 270 days at 25 °C. Corrosion products were identified through XRD and Mössbauer spectroscopy. The X-ray diffraction patterns were obtained by using a Siemens D500 diffractometer equipped with a copper anode X-ray tube; irradiation with a diffracted beam monochromator (Kα = 1.5405 Å) covered a 2θ diffraction angle ranging from 10 to 85° in steps of 0.02^{o}. Mössbauer spectra were taken at 300 K with a conventional spectrometer operated in transmission geometry and triangular mode. The source was ^{57}Co in a Rh matrix with activity of 925 MBq (25 mCi). The velocity scale and all the data are referred to a metallic α-Fe absorber at 300 K. The absorption spectra were fitted by the NORMOS software [34]. Diffuse reflectance ultraviolet-visible (DRUV) spectroscopy was performed using an Evolution 600 spectrometer with temperatures ranging from 50 to 150 °C.

2.4. Polarization measurements

Electrochemical measurements were carried out in a standard-three-electrode cell. The counter electrode was a graphite cylindrical bar; the reference electrode consisted of a commercial saturated calomel electrode (SCE) with a Luggin capillary probe, and the working electrode made of X52 steel was supported into a cylindrical Teflon bar. Tests were performed in naturally aerated PW at 25 and 45 °C from 8 to 96 days without stirring. The electrochemical tests were performed in a potentiostat/galvanostat PGSTAT302N controlled by a PC through the NOVA 2.1 software. Polarization scans were carried out at ± 250 mV in reference to the open circuit potential (OCP) measured by a Saturated Calomel Electrode (SCE) at a scan rate of 0.166 mV s^{-1}.

3. RESULTS AND DISCUSSION

3.1. X-ray photoelectron spectroscopy

Figure 1 shows the survey spectrum of the steel in contact with PW after 60 days, in which, peaks corresponding to O, Cl, Fe, Na, Ca, C, and S are observed [35]. The signal intensities of Fe, Cl and O were associated with the corrosion products formed on the steel surface (Table 2). The presence of carbon was related to the presence of oil traces in the PW, which were adsorbed on steel. The relatively high concentration of chloride on the steel surface was ascribed to the presence of sodium,

calcium and iron salts in water. It is evident that the amounts of iron and oxygen present in the steel exposed to PW allow the formation of Fe^{3+} oxyhydroxide products on the external part of the formed layer.

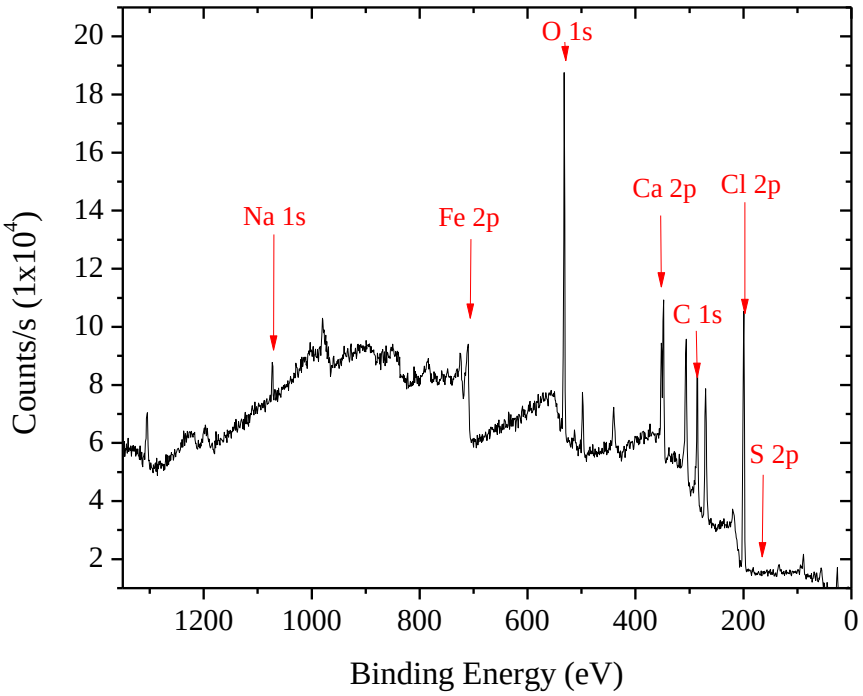

Figure 1. XPS spectrum of X52 steel exposed to PW for 60 days.

Table 2. Atomic percent of elements on X52 steel exposed to PW for 60 days.

Atomic percent (%)	Level 0*	Level 6**
C 1s	30.4	13.6
O 1s	27.5	18.38
Cl 2p	23.7	27.09
Fe 2p	8.1	21.87
Ca 2p	7.8	10.12
Na 1s	2.5	8.73
S 2p	0.0	0.22

Where (*) represents the atomic percent of each element present on the metal surface calculated before pickling the surface with argon ions; (**) refers to the atomic percent of the elements present on the metal surface calculated after the pickling process.

Figure 2 shows the signal of the elements at the end of the sputtering process of the steel surface (level 6) that was exposed to PW for 60 days. An increase in the Fe 2p and Na 1s signals was observed whereas those for O 1s and C 1s decreased. The atomic percentage variations of the elements found during the sputtering process are shown in Figure 3. It is observed that at level 6, the atomic

percentage of Fe 2p was increased because of the steel matrix nearness while both O 1s and C l s decreased. Ferric oxyhydroxides and the spinel type of iron oxides such as magnetite, which forms the external corrosion layer, are assumed to be products derived from oxygen reduction. An increase in the intensity of the sodium signal is detected as a consequence of the sputtering process, which might indicate that the inorganic salt competed with either hydroxyl or hydronium ions for the metal surface, as they are part of the complex layer that covers the steel surface in the corrosive environment [36].

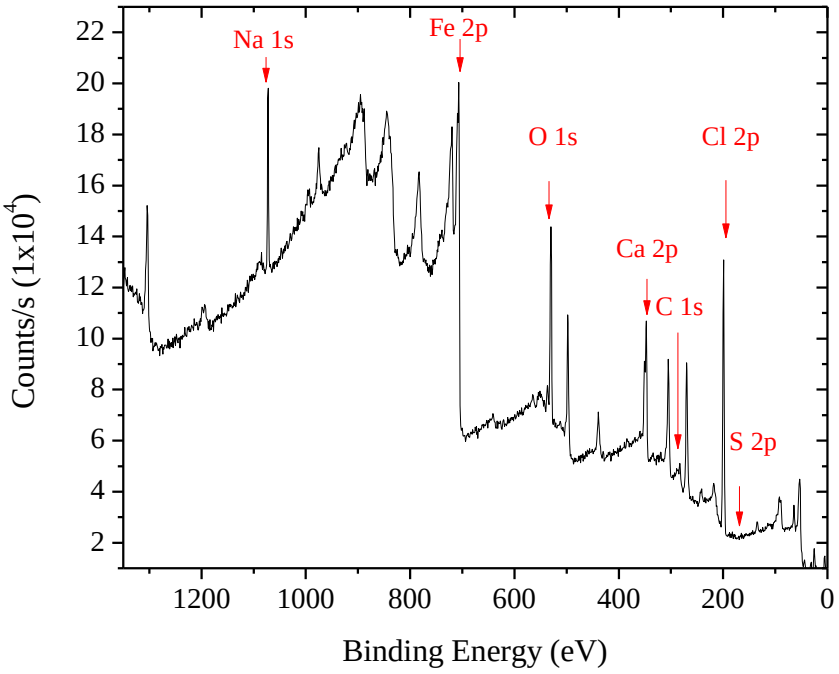

Figure 2. XPS spectrum of X52 steel, exposed to PW for 60 days, at the end of the sputtering process (level 6)

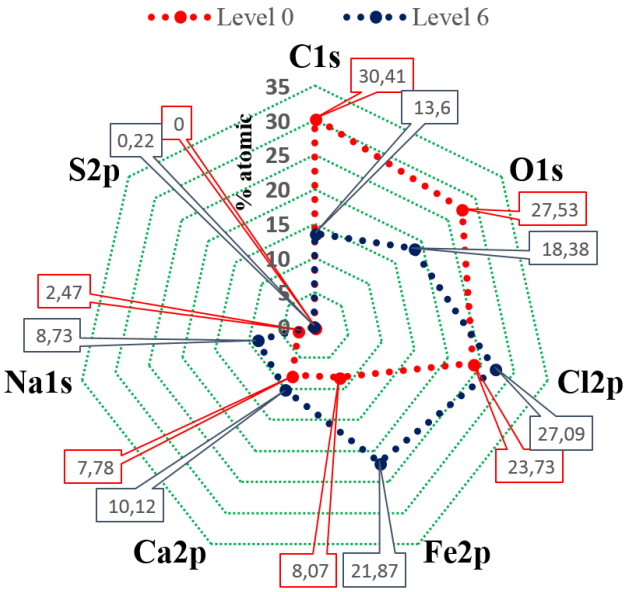

Figure 3. Depth profile of elements present on X52 steel exposed to PW for 60 days at the beginning (level 0) and end of the sputtering process (level 6).

Figure 4 shows the high resolution spectrum of Fe 2p, where the main doublet located at the 708.9 (Fe $2p_3$) and 722.4 (Fe $2p_1$) eV regions with their corresponding satellite structures at 715 (Fe $2p_3$) and 728.8 (Fe $2p_1$) eV represents the iron oxidation state (II). Iron in the aggressive medium produces Fe^{2+} ions that normally at pH values close to neutrality form iron hydroxides ($Fe(OH)_2nH_2O$); these are transformed into "green rust" by the effect of hydrolysis and/or oxidation [37]. The shape and location of peaks at 711.1 and 723.8 eV indicate the presence of Fe^{3+}, which can be characterized by ferric oxyhydroxides (FeOOH) (FeOOH) such as lepidocrocite, goethite and magnetite (Fe_3O_4). In addition, two types of iron salts such as $FeCl_2$ (located at 710.3 and 729.0 eV) and iron sulfates (located 712.8 and 726.3 eV) were identified at low concentrations on the surface.

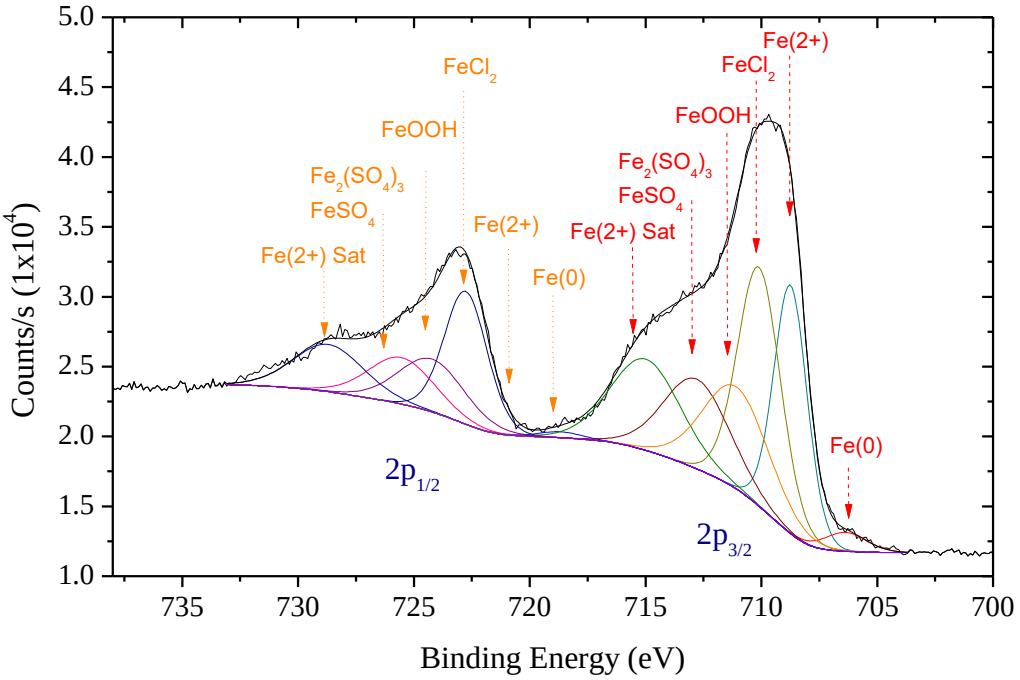

Figure 4. High resolution (Fe 2p) XPS spectrum of X52 steel exposed to PW for 60 days at the beginning (level 0) of the sputtering process.

Finally, the energy peaks located at 706.5 and 719.4 eV are characteristic of metallic iron (Fe^0) [34]. Figure 5 shows the atomic percent profile of Fe 2p, which depends on the sputtering process. The atomic percentage of metallic iron was increased drastically with depth due to the vicinity of the steel matrix (Figure 6). The concentrations of oxyhydroxide complexes of Fe^{3+}(FeOOH) and Fe^{2+} chlorides ($FeCl_2$) decreased, which indicates that such complexes are part of the external layer of the whole cluster of production products. Two signals at 710.1 and 722.4 eV were ascribed to iron salts in the form of chlorides ($FeCl_2$) while iron sulfates were formed at lower concentrations on the surface, located at 713.3 and 725.6 eV, were identified. Finally, the energy peaks at 706.4 and 719.1 eV are characteristic of metallic iron (Fe^0) with an atomic percentage of 8.8 %. The element profile suggested that either Cl^- anions or sodium/calcium chlorides were firstly adsorbed on the steel surface along with water molecules so the formation of ($Fe(OH)_2nH_2O$) occurred. This process is apparently followed by

iron oxidation from Fe^{2+} to Fe^{3+}, leading to the formation of both iron oxyhydroxides (FeOOH) and magnetite Fe_3O_4 at the solid/liquid interphases [38]. In addition, the behavior of the atomic percent profile of iron chloride ($FeCl_2$) helps establish the occurrence of Fe^{2+} cations through the layer of corrosion products. XPS also displays the presence of $FeSO_4$ [39], which lowers water pH as:

$$Fe^{2+}_{(ac)} + SO_4^{2-} \rightarrow FeSO_4 \quad (1)$$

$$4FeSO_4 + 6H_2O + O_2 \rightarrow 4FeOOH + 4H_2SO_4 \quad (2)$$

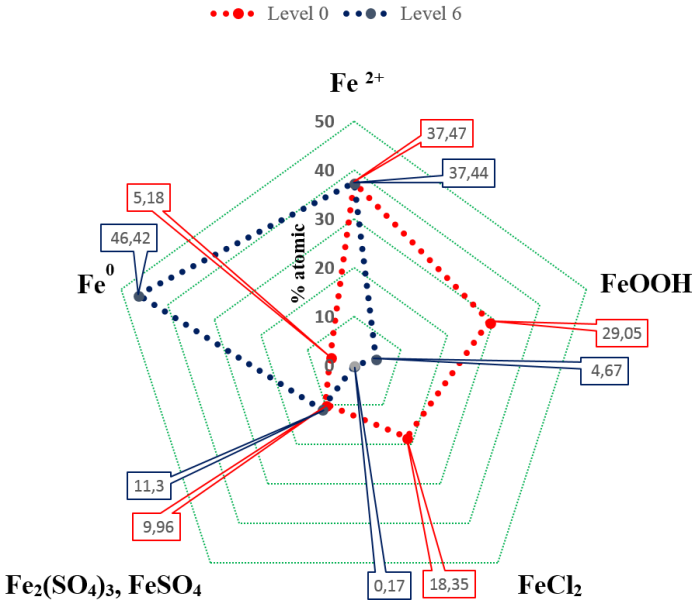

Figure 5. Depth profile (Fe 2p) of X52 steel exposed to PW for 60 days at the beginning (level 0) and end of the sputtering process (level 6).

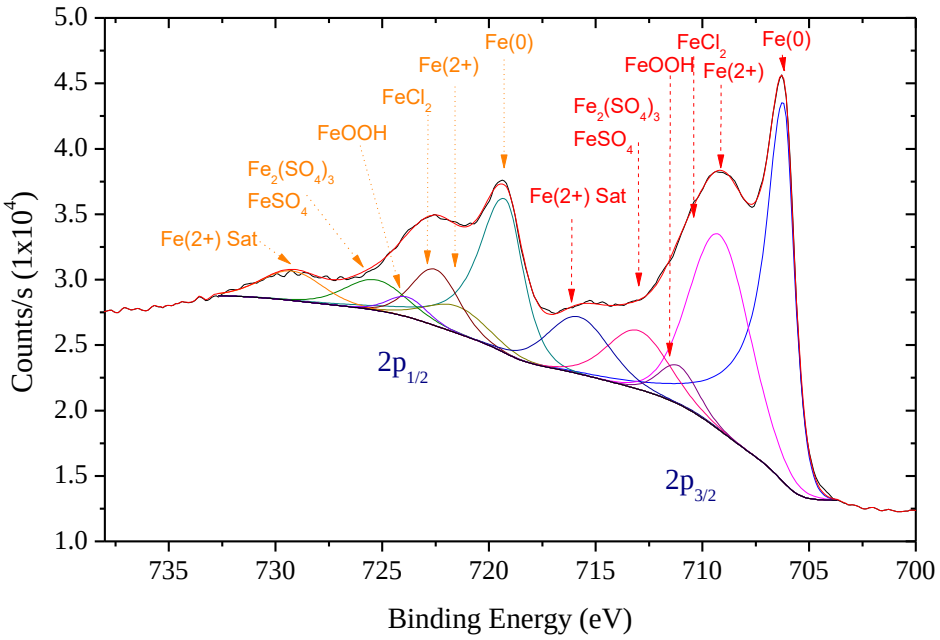

Figure 6. High resolution XPS spectrum of X52 steel exposed to PW for 60 days at the end (level 6) of the sputtering process.

3.2. UV-vis spectroscopy

The surfaces exposed to PW for 90, 180 and 270 days at 25 °C showed a heterogeneous surface with a high concentration of corrosion products. It is assumed that the sample with 270 days of immersion is representative for the identification of corrosion products as it contained the amount and variety of those found on steel in PW for other testing times. The reflectance spectrum shows that lepidocrocite, (α-FeO(OH)) was the main corrosion product formed in the surface external layer after a long exposure time to the aggressive medium (Figure 7). No other signals for another chemical species were found, probably because of low concentration and signal transposition with dominant compounds. The characteristic signal of lepidocrocite is in good agreement with the work reported by Torrent & Barron [40] in which 500-nm-oxide powders were analyzed.

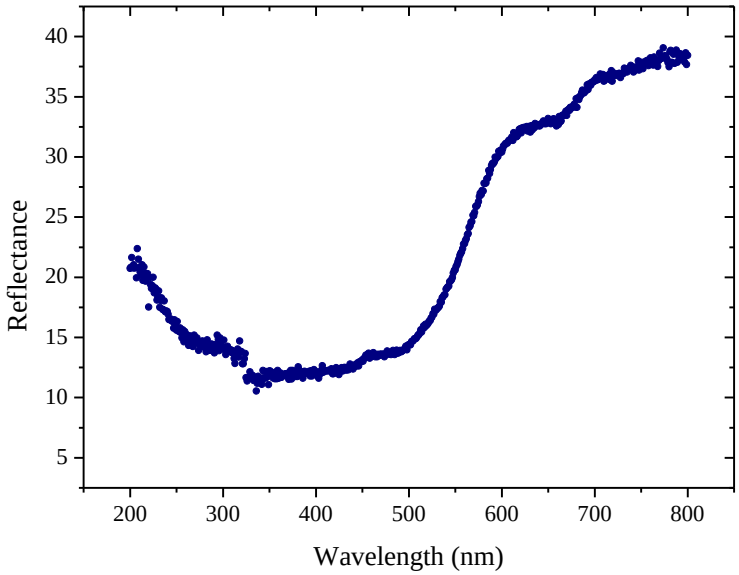

Figure 7. DRUV spectrum of the corrosion products formed on X52 steel after 270 days in PW.

3.3. X-ray diffraction (XRD)

Figures 8 (a), (b) and (c) show the XRD spectra obtained for the corrosion products at 90, 180 and 270 days at 25 °C. Figures 8 (a-b) show the presence of two high-intensity signals, which are ascribed to sodium chloride [05-0628 card (JCPDS)] and lepidocrocite ($Fe^{3+}O(OH)$) [44-1415 card]. The high intensity signal of sodium chloride masks the low-intensity signals obtained within the 2θ interval ranging from 10 to 30, which corresponds to lepidocrocite [41, 42]. In Figure 8 (c), at 270 days, the changes are evident in comparison with the previously analyzed samples. The high concentration of sodium chloride affected the intensity of iron compound signals, although it is still possible to clearly identify those attributed to lepidocrocite and magnetite, which can be formed through a slow oxidation process, according to the 88-0866 card. Likewise, the oxidation state of iron changed from Fe^{2+} to Fe^{3+} as a natural oxidation of steel immersed in the corrosive medium for such long periods of times, as it was later confirmed by Mössbauer spectroscopy.

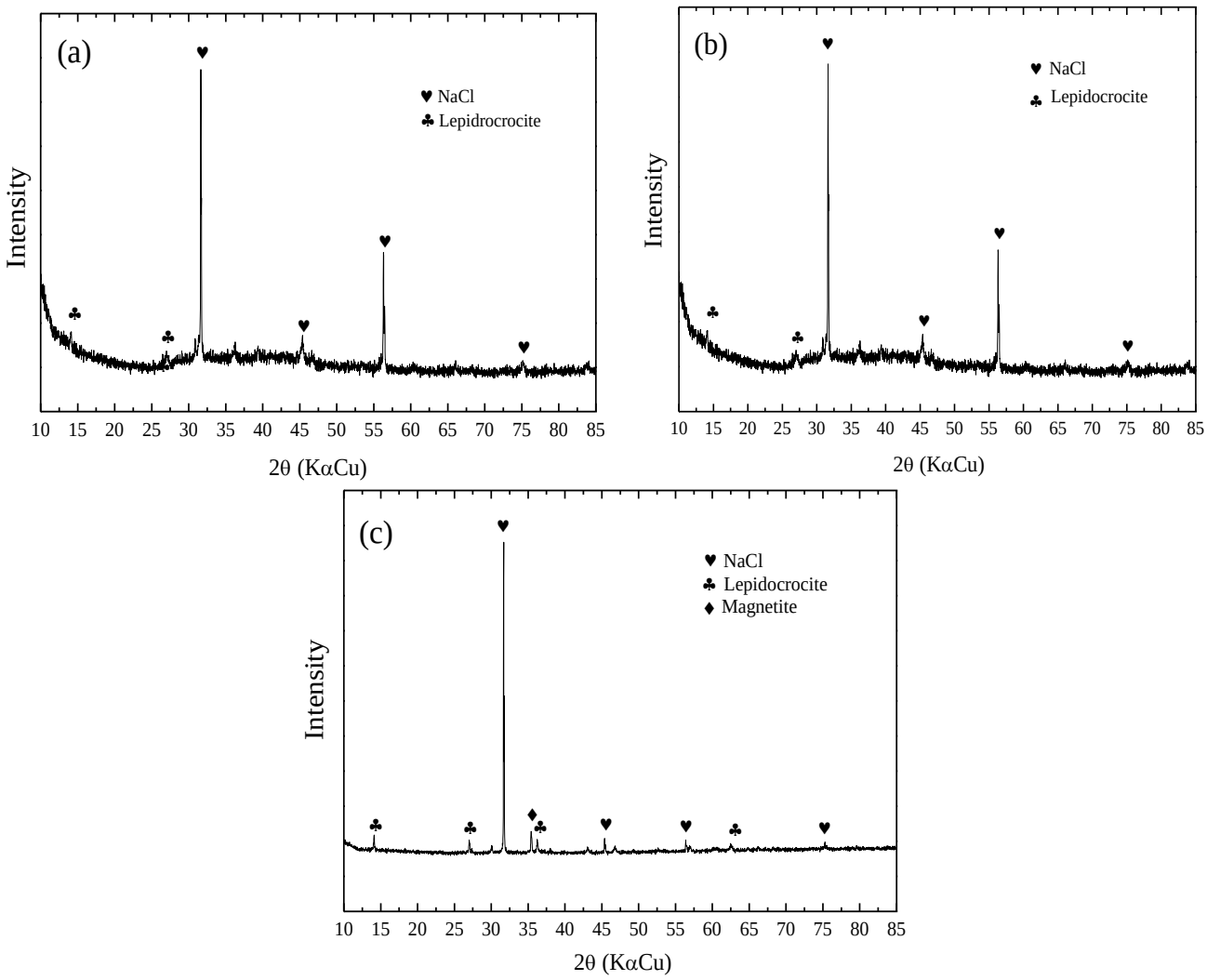

Figure 8. XRD patterns of X52 steel immersed in PW after a) 90 days, b) 180 days and c) 270 days.

3.4. Mössbauer spectroscopy

The spectra of the samples exposed to PW for different times are shown in Fig. 9(a). After 90 days of immersion, the spectrum displays two main doublets that agree with the formation of lepidocrocite at 100 % (Table 3). Figure 9 (b) shows the spectra of the corrosion products after 180 days of exposure to PW, which were fitted to a magnetic sextet and two paramagnetic doublets. The low intensity magnetic sextet indicates the presence of goethite whereas the two main doublets correspond to the akaganeite/lepidocrocite phase ($Fe^{3+}O(OH)$). The corrosion products formed after the immersion of steel in PW for 270 days show important changes in comparison with those samples after 90 and 180 days. As shown in Figure 9 (c), oxyhydroxide phases such as lepidocrocite (γ-FeOOH) and magnetite (Fe_3O_4) are present and predominated over goethite (α-FeOOH).

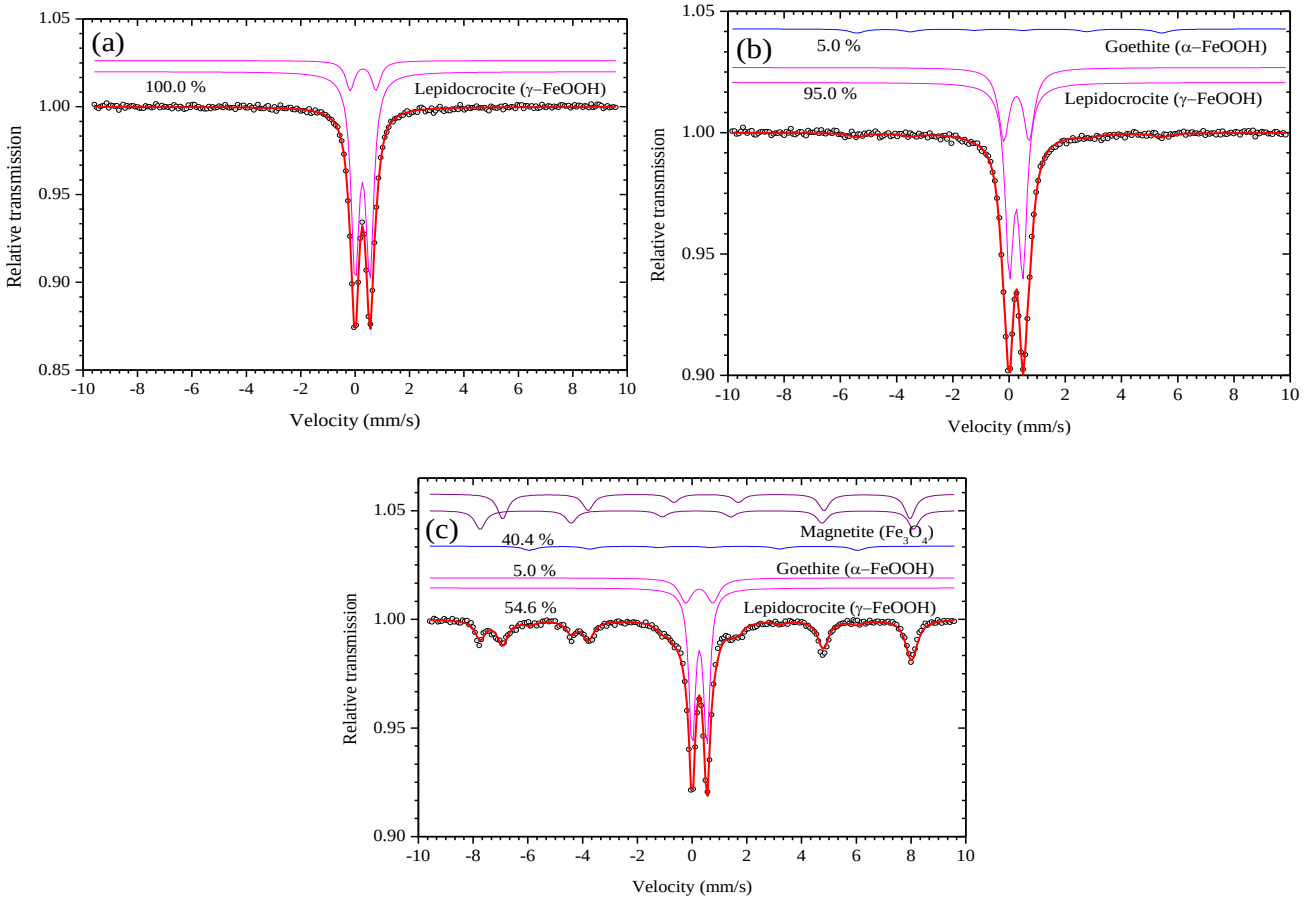

Figure 9. Mössbauer spectra of the corrosion products formed on X52 steel immersed in PW for a) 90 days, b) 180 days and c) 270 days.

Table 3. Mössbauer characterization of corrosion products formed on X52 steel exposed to PW.

Days	Chemical species	δ (mm s^{-1})	Δ (mm s^{-1})	BHF (Teslas)	Spectral area (%)
90	(γ-FeOOH)	0.26	0.56	--	100.0
		0.27	0.97	--	
180	(α-FeOOH)	0.32	0.59	34.0	5.0
	(γ-FeOOH)	0.25	0.57	--	95.0
		0.26	0.97	--	
270	Fe_3O_4	0.17	0.01	49.0	40.4
		0.51	0.01	46.1	
	(α-FeOOH)	0.19	0.32	36.0	5.0
	(γ-FeOOH)	0.27	0.57	--	54.6
		0.26	0.98	--	

Where: δ = isomer shift relative to α-Fe at RT; Δ = quadrupole splitting; BHL = hyperfine magnetic field. Error: δ = ±0.01 mm/s; Δ = ±0.01 mm/s; BHF=±0.2 T.

3.5. Polarization measurements

Figures 10 (a) and (b) show the behavior of mild steel after polarization testing as a function of immersion time and temperature (25 and 45 °C) in PW. After 8 days, it is observed that the

potentiodynamic curves of the material passed from a relatively high current density (78-44 µA cm^{-2}) to a lower value within 16-40 h (6-13 µA cm^{-2}). This parameter increased again from 20 to 69 µA cm^{-2} in the 48-64 h interval at 45 °C, then decreased (72-80 h) and increased again (88-96 h), showing higher corrosion rates as temperature rises. Temperature boosted the corrosion kinetics and mass transfer by providing energy to the corrosion process [43, 44]. This behavior is similar at 25 °C though the corrosion current density (i_{corr}) changed roughly from high to low every 8 h (Table 4).

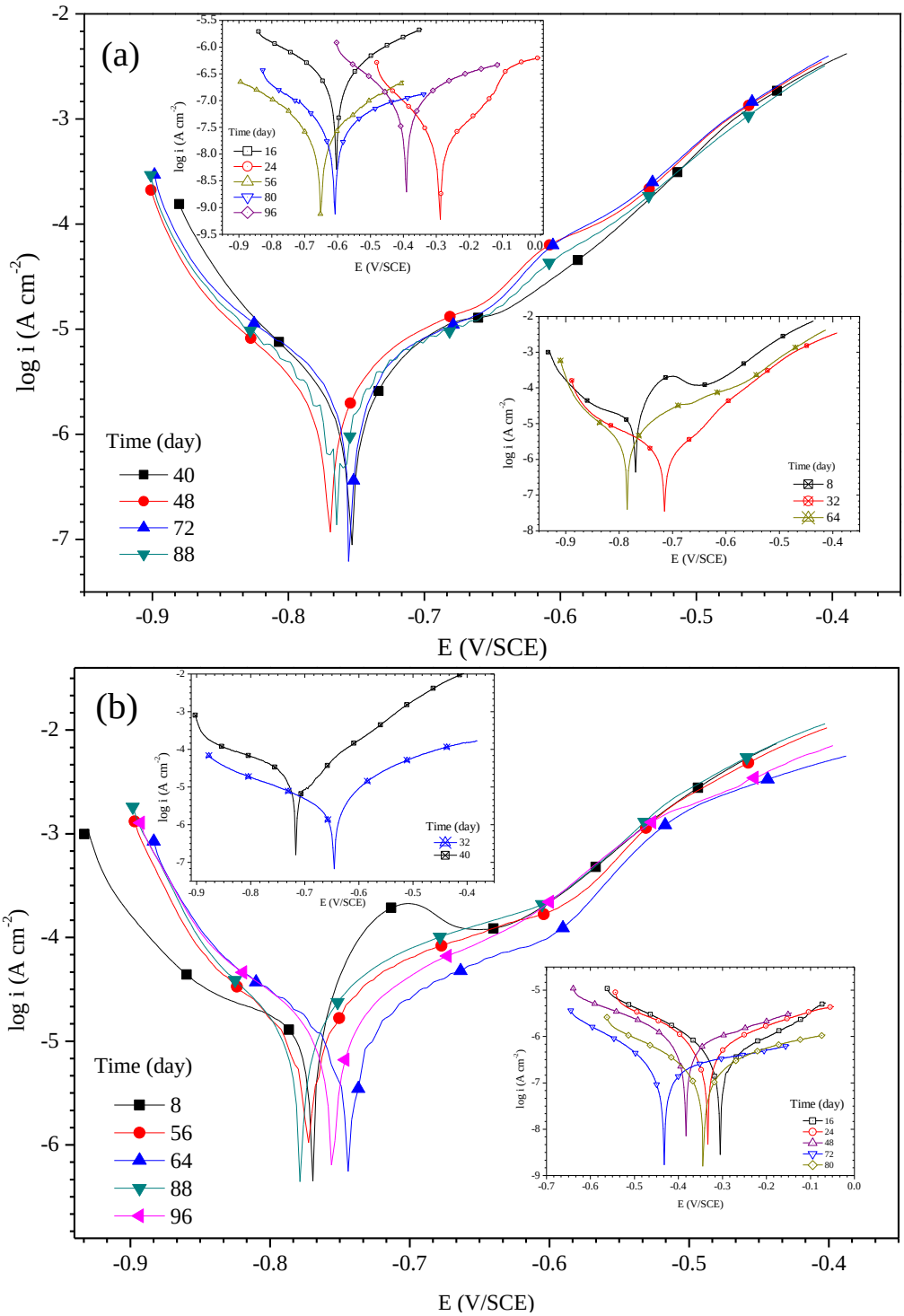

Figure 10. Potentiodynamic polarization curves of X52 steel in PW at different immersion times and temperatures of a) 25 °C and b) 45 °C.

These changes in current density are ascribed to the formation/removal of corrosion products from the metallic surface under corrosion. A particular feature is shown by those curves displaying relatively high current densities (10^{-5}-10^{-4} A cm^{-2}), in which an abrupt change in the anodic branch is observed; this effect is commonly assigned to the formation/removal of corrosion products by the effect of time and temperature [45]. The polarization curves indicated that the oxidation reaction is affected by the layers of iron compounds and salts deposited on the metallic surface. An important feature is the porosity of the layer that allows the continuous diffusion of aggressive chemical species through the metal-corrosion product interface affecting Fe dissolution.

Table 4. Electrochemical parameters of X52 steel at 25 °C after exposure to PW for 8-96 days.

Days	$-\beta_c$ (mV dec^{-1})	β_a (mV dec^{-1})	$-E_{corr}$ vs. SCE (mV)	i_{corr} (μA cm^{-2})	V_{corr} (mm y^{-1})
8	268	141	770	44	0.5112
16	234	277	604	7	0.0813
24	205	255	290	6	0.0697
32	133	117	715	9	0.1045
40	104	96	754	13	0.1510
48	122	116	770	27	0.3136
56	132	123	651	30	0.3485
64	95	84	785	31	0.3601
72	159	192	754	23	0.2672
80	126	161	608	20	0.2323
88	141	151	764	14	0.16264
96	326	213	392	5	0.0580

Table 5 shows reported electrochemical parameters such as i_{corr}, corrosion potential (E_{corr}), corrosion rate (V_{corr}), and anodic and cathodic Tafel slopes (β_a and β_c). The i_{corr} changes are associated with an adsorption-desorption process that affects the corrosion products and consequently the corrosion rate. This parameter depends on the temperature and time exposing steel to PW. By analyzing the E_{corr} data and taking the E_{corr} at 8 days as a reference, it was observed that at 25 and 45 °C, these values tend to be displaced towards more active potentials due to the oxidation process, which favor the corrosion process [46, 47]. Figure 11 shows the behavior of i_{corr} at 25 and 45 °C, where the highest values occurred at 45 °C. An increase in temperature increases both the electrochemical reaction kinetics and oxygen solubility, which in turn augment the corrosion rate as indicated by Arrhenius equation [48]. At some specific times, the changes in i_{corr} tend to be lower because of the formation of corrosion products, mainly of Fe_xO_y and FeOOH, which make more difficult the diffusion of ions such as Cl^-, OH^- and SO_4^{2-} to the steel surface, resulting in a lower corrosion rate [49]. Lower current density values corroborate that active sites are blocked, mainly by

oxide films, so the corrosion rate is controlled by the formation/removal of oxides on the metallic surface [50], where such process is more evident at 45 °C, in which i_{corr} underwent remarkable changes, increasing the corrosion rate after passivation breakdown.

Table 5. Electrochemical parameters of X52 steel at 45 °C after exposure to PW for 8-96 days.

Days	$-\beta_c$ (mV dec^{-1})	β_a (mV dec^{-1})	$-E_{corr}$ vs. SCE (mV)	i_{corr} (µA cm^{-2})	V_{corr} (mm y^{-1})
8	37	243	767	78	0.9061
16	286	245	306	6	0.0697
24	370	223	335	5	0.0581
32	106	259	646	21	0.2439
40	102	103	704	65	0.7551
48	123	271	386	74	0.8597
56	115	153	776	78	0.9062
64	194	183	752	69	0.8016
72	128	149	430	60	0.6970
80	135	121	349	51	0.5925
88	122	152	779	54	0.6273
96	167	171	762	72	0.8364

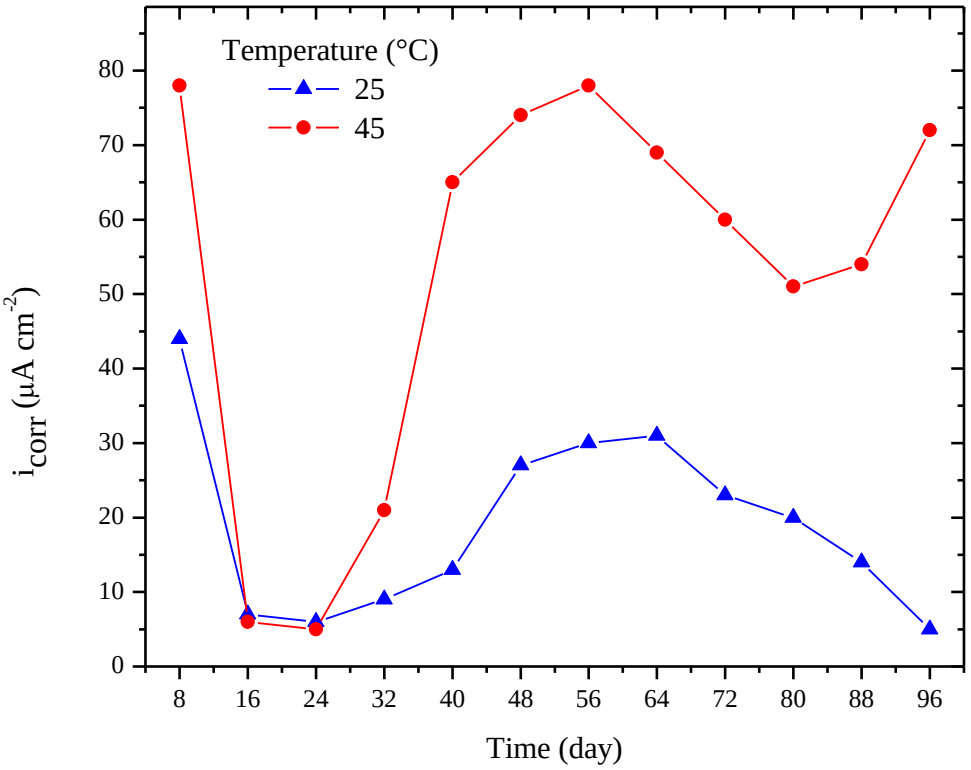

Figure 11. Corrosion current density, i_{corr}, of X52 steel at 25 and 45 °C in PW

3.6. SEM/EDX analysis

Figure 12 shows the steel surface after 90 days of immersion in PW at 25 °C, in which the presence of NaCl is observed. After 180 days, Figure 13 shows the presence of a thick layer of corrosion products interspersed with salts such as sodium chloride and some calcium chloride ($CaCl_2$), which is in agreement with the elements detected by the EDX analysis and PW chemical composition (Table 1). After 270 days, Figure 14, the concentration of oxygen and iron increased, where these elements partially constituted the porous layer of the corrosion products on the metal surface. Other salts of sulfates and nitrates were not detected, although the plasma emission analysis confirmed their presence, probably as a result of a biased surface concentration and minor contents.

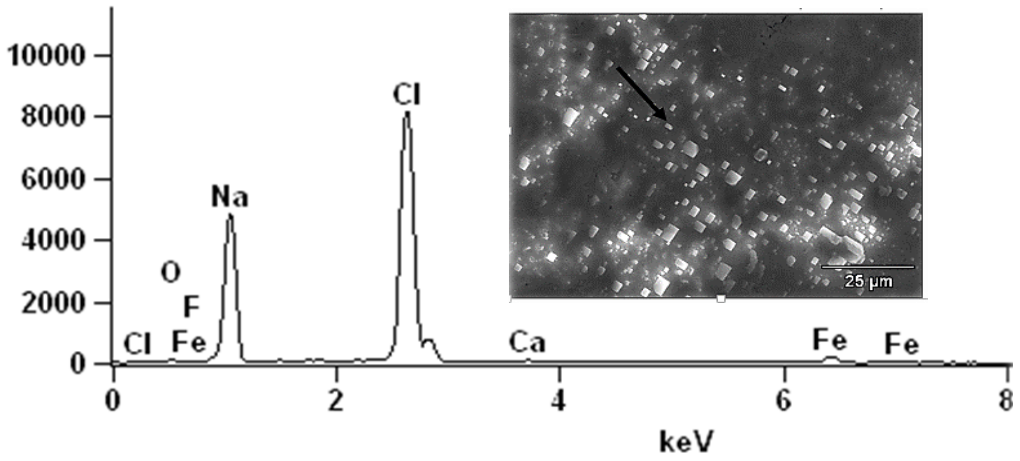

Figure 12. SEM-EDX analysis of X52 steel after 90 days of immersion in PW at 25 °C, showing the presence of solid precipitates of NaCl (1000X).

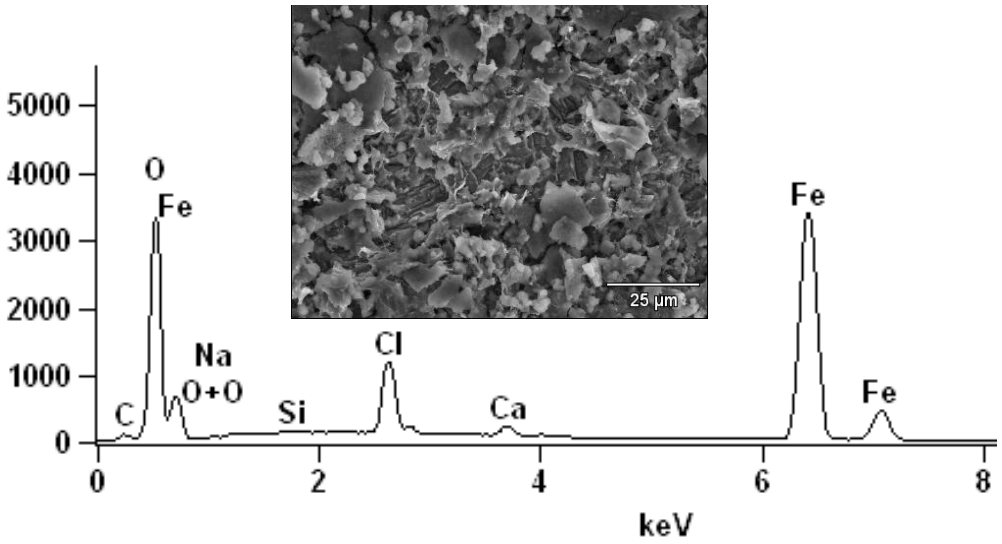

Figure 13. SEM-EDX analysis of X52 steel after 180 days of immersion in PW at 25 °C, showing the presence of corrosion products containing solid salts of sodium chloride and calcium chloride (1000X)

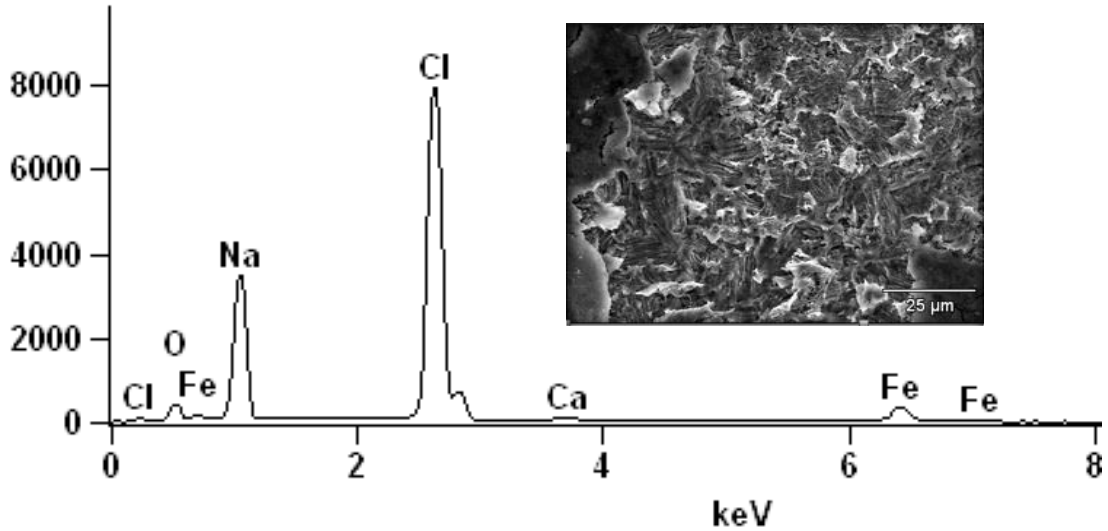

Figure 14. SEM-EDX analysis of X52 steel after 270 days of immersion in PW at 25 °C, showing localized corrosion under corrosion deposits and sodium chloride salt

The steel surface, after 270 days, showed a porous microstructure with the deposition of salts (NaCl) evidenced by the presence of Na and Cl and possibly of corrosion products ($FeCl_2$) as reported by the XPS analysis. The steel sample also showed localized corrosion (Figure 14) caused by the high concentration of Cl^- ions in combination with long exposure times [49].

3.7. Corrosion mechanism of X52 in PW

Ferrous hydroxide is a relatively insoluble solid phase and under anaerobic conditions, at relatively low temperature, iron hydroxide can be transformed into magnetite [51]. Nevertheless, in our case, rust (Fe_2O_3) in the anodic dissolution of iron is balanced by the cathodic reaction of Fe (III). According to the XRD and Mössbauer analyses, magnetite appears after the formation of oxyhydroxides such as lepidocrocite (γ-FeOOH) and goethite (α-FeOOH), which promoted the oxidation of Fe^{2+} to Fe^{3+}, forming a spinel type of iron oxide, which can promote once again a reoxidation to ferric oxyhydroxides [30]. This explains the presence of goethite and magnetite in the corrosion products after prolonged exposure (270 days) of the metal to the aqueous medium.

$$Fe^{2+} + 8FeOOH + 2e^- \rightarrow 3Fe_3O_4 + 4H_2O \quad (3)$$

$$3Fe_3O_4 + \tfrac{3}{4}O_2 + \tfrac{9}{2}H_2O \rightarrow 9FeOOH \quad (4)$$

Some studies have explained that the corrosion process in steel exposed to a corrosive medium produces Fe^{2+} ions, which are transformed into "green rust" by hydrolysis and/or an oxidation effect with the following general formula [37, 51]:

$$Fe_xO_y(OH)_zYxH_2O \qquad \text{where } Y = Cl^-, Br^-, SO_4^{2-} \quad (5)$$

On the anodic sites, the iron dissolution not only depends on the OH^- ions, but also on other anions such as Cl^- ions [52]. Studies on the metal dissolution at the anodic branch were done by Kolotyrkin *et al.* [53] who proposed that at a first stage, the water molecules react instead of the OH^- ions, which is more feasible for media with pH values below 5:

The metal hydroxide $(FeOH)_{ads}$ is unstable and can react with chlorides or bisulfates or can be transformed into corrosion products of the iron hydroxide "green rust" type, which are oxidized to oxyhydroxides according to the following reaction:

$$Fe(OH)_2(H_2O)_{n-1} + Fe(OH)Cl(H_2O)_{n-1} + H^+ \xrightarrow{\frac{1}{2}O_2} FeOOH + nH_2O + Cl^- \quad (6)$$

Based on the results obtained from the analysis of corrosion products by the Mössbauer, XRD, XPS and SEM techniques and the electrochemical studies as well, it is proposed that the external layers, consisting of oxyhydroxides, are partially detached from the metal surface after magnetite formation, which is dissolved/removed to allow further diffusion of ions from the aggressive medium to the metallic surface to reinitiate the corrosion process, which might be related to the fluctuations observed in the potentiodynamic tests.

4. CONCLUSIONS

XPS analyses established that chloride ions and water molecules were adsorbed firstly on the metal surface, forming $Fe(OH)_2n(H_2O)$ and $Fe(OH)Cl(H_2O)_n$ complexes, which started a sequential oxidation process from Fe^{2+} to Fe^{3+}, producing lepidocrocite, goethite and later magnetite on the external layer of the corrosion products.

Mössbauer spectra showed that the corrosion products corresponded to lepidocrocite (γ-FeOOH), goethite (α-FeOOH) and magnetite (Fe_3O_4). XRD confirmed the formation of lepidocrocite and magnetite in the outer layer that can be detached from the metal surface, while UV-vis spectroscopy only detected the presence of lepidocrocite on the metallic surface.

The corrosion behavior of carbon steel in PW was affected by time and temperature; the steel surface condition changed from an active to a passive state, so corrosion was controlled by a diffusion process of chemical species in the medium and corrosion decreased when the surface was completely covered by corrosion products. Temperature favored mass transfer so the corrosion rate changed every 8 days at 25 °C, and every 48 days at 45 °C. In both cases, E_{corr} tended to be displaced towards more active potentials, favoring corrosion.

Scanning electron microscopy indicated that general and localized corrosion occurred on the metallic surface; one derived from aqueous corrosion and the other from the high concentration of chlorides. The layers of corrosion products were not compact and facilitated the diffusion of ions into the metal/oxide interface in the PW despite the fact that lepidocrocite is relatively protective.

ACKNOWLEDGEMENTS
We thank M. Corrales for the technical support and Conacyt-Mexico for the scholarship provided. OOX thanks SNI, BUEP-VIEP. PAL thanks SENER-CONACYT-HIDROCARBUROS.

References

1. M. Bader, *Desalination,* 208 (2007) 159.
2. L. Torres, O. P. Yadav, E. Khan, *Sci. Total Environ.*, 539 (2016) 478.
3. Q. Huang, F. Mao, X. Han, J. Yan, Y. Chi, *Fuel,* 118 (2014) 214.
4. G. T. Tellez, N. Nirmalakhandan, J. L. Gardea-Torresdey, *Adv. Environ. Res.*, 6 (2002) 455.
5. H. Tan, W. Rao, H. Ma, J. Chen, T. Li, *J. Asian Earth Sci.*, 40 (2011) 651.
6. S. Mondal, S. R. Wickramasinghe, *J. Membr. Sci.*, 322 (2008) 162.
7. K. S. Sorbie, E. J. Mackay, *J. Pet. Sci. Eng.*, 27 (2000) 85.
8. M. A. Migahed, M. A. Hegazy, A. M. Al-Sabagh, *Corros. Sci.*, 61 (2012) 10.
9. S. S. M. Tavares, J. M. Pardal, F. B. Mainier, et al., *Eng. Failure Anal.*, 61 (2016) 100.
10. A. B. Carpenter, Origin and chemical evolution of brines in sedimentary basins, SPE Annual Fall Technical Conference and Exhibition, Society of Petroleum Engineers, Houston, Texas, 1978,
11. L. S. Land, G. Macpherson, *AAPG Bulletin,* 76 (1992) 1344.
12. Z. Hu, D. Duan, S. Hou, X. Ding, S. Li, *J. Mater. Sci. Technol.*, 31 (2015) 1274.
13. B. Dong, Y. Xu, H. Deng, F. Luo, S. Jiang, *Desalination,* 326 (2013) 141.
14. O. Shabarchin, S. Tesfamariam, *J. Loss Prev. Process Ind.*, 40 (2016) 479.
15. Y. Liu, B. Zhang, Y. Zhang, L. Ma, P. Yang, *Eng. Failure Anal.*, 60 (2016) 307.
16. M. Deyab, *Corros. Sci.*, 49 (2007) 2315.
17. H. Tian, W. Li, B. Hou, D. Wang, *Corros. Sci.*, 117 (2017) 43.
18. S. Nešić, *Corros. Sci.*, 49 (2007) 4308.
19. H. Mansoori, R. Mirzaee, A. Mohammadi, Pitting corrosion failures of natural gas transmission pipelines, IPTC 2013: International Petroleum Technology Conference, 2013,

20. Y.-S. Choi, S. Nešić, *Int. J. Greenhouse Gas Control*, 5 (2011) 788.
21. G. Zhang, Y. Cheng, *Electrochim. Acta*, 56 (2011) 1676.
22. G. A. Zhang, Y. F. Cheng, *Corros. Sci.*, 51 (2009) 87.
23. C. Sun, J. Sun, Y. Wang, et al., *Corros. Sci.*, 107 (2016) 193.
24. Y. Hua, R. Barker, A. Neville, *Int. J. Greenhouse Gas Control*, 37 (2015) 412.
25. E. Gulbrandsen, J. Kvarekvål, H. Miland, *Corrosion*, 61 (2005) 1086.
26. R. L. Martin, Corrosion Consequences of Oxygen Entry into Oilfield Brines, Corrosion 2002, NACE International, Denver, Colorado, 2002,
27. N. Sridhar, D. S. Dunn, A. M. Anderko, M. M. Lencka, H. U. Schutt, *Corrosion*, 57 (2001) 221.
28. M. J. Schofield, K. Waterton, T. Evans, P. I. Nice, Corrosion Behavior of Carbon Steel, Low Alloy Steel and CRA's in Partially Deaerated Sea Water and Commingled Produced Water, Corrosion 2004, NACE International, New Orleans, Louisiana, 2004,
29. X. Zhu, G. Huang, L. Lin, D. Liu, *Corros. Eng., Sci. Technol.*, 43 (2008) 328.
30. Y. Wang, G. Cheng, W. Wu, Q. Qiao, Y. Li, X. Li, *Appl. Surf. Sci.*, 349 (2015) 746.
31. M. Deyab, *Austin Chem Eng.*, 1 (2014) 1010.
32. U. S. EPA. (2014) Method 6010D (SW-846): Inductively Coupled Plasma-Atomic Emission Spectrometry. Revision 4. Washington, DC.
33. R. A. J. Pisigan, J. E. Singley, *Mater. Perform.*, 24 (1985) 26.
34. R. A. Brand (1987) Normos Mossbauer Fitting Program. The Normos program is available from Wissel GmbH. D-82319 Starnberg. Germany Starnberg.
35. C. D. Wagner, D. M. Bickham (1989) NIST X-ray Photoelectron Spectroscopy Database V.1.0 New York.
36. K. D. Bomben, J. Chastain, J. F. Moulder, P. E. Sobol, W. F. Stickle, Handbook of X-ray Photoelectron Spectroscopy. Perkin-Elmer Corporation, (1992) Minnesota.
37. Y. Tamaura, *Inorg. Chem.*, 24 (1985) 4363.
38. S.-K. Kwon, S. Suzuki, M. Saito, Y. Waseda, *Corros. Sci.*, 48 (2006) 3675.
39. Y.-S. Choi, S. Nesic, D. Young, *Environ. Sci. Technol.*, 44 (2010) 9233.
40. J. Torrent, V. Barrón, *Encycl. Surf. Colloid Sci.*, 1 (2002) 1438.
41. U. Schwertmann, R. M. Taylor, *Clays Clay Miner.*, 20 (1972) 151.
42. S. K. Kwon, S. Suzuki, M. Saito, T. Kamimura, H. Miyuki, Y. Waseda, *Corros. Sci.*, 48 (2006) 1571.
43. Y. Lu, H. Jing, Y. Han, L. Xu, *Mater. Chem. Phys.*, 178 (2016) 160.
44. M. P. Desimone, G. Gordillo, S. N. Simison, *Corros. Sci.*, 53 (2011) 4033.
45. F. E.-T. Heakal, A. Fouda, M. Radwan, *Mater. Chem. Phys.*, 125 (2011) 26.
46. I. B. Obot, E. E. Ebenso, M. M. Kabanda, *J. Environ. Chem. Eng.*, 1 (2013) 431.
47. M. W. S. Jawich, G. A. Oweimreen, S. A. Ali, *Corros. Sci.*, 65 (2012) 104.
48. Y. Wang, G. Cheng, Y. Li, *Corros. Sci.*, 111 (2016) 508.
49. D. Asefi, M. Arami, N. M. Mahmoodi, *Corros. Sci.*, 52 (2010) 794.
50. C. Verma, M. A. Quraishi, A. Singh, *J. Taiwan Inst. Chem. Eng.*, 58 (2016) 127.
51. T. Peev, V. Taseva, A. Akala, *Mater. Corros.*, 44 (1993) 62.
52. S. Réguer, P. Dillmann, F. Mirambet, *Corros. Sci.*, 49 (2007) 2726.
53. Y. M. Kolotyrkin, V. V. Losev, A. N. Chemodanov, *Mater. Chem. Phys.*, 19 (1988) 1.